

Article

# Nanosecond Laser Fabrication of Dammann Grating-like Structure on Glass for Bessel-Beam Array Generation

Prasenjit Praharaj<sup>1,2</sup>  and Manoj Kumar Bhuyan<sup>1,2,\*</sup>

<sup>1</sup> CSIR—Central Scientific Instruments Organisation, Sector 30C, Chandigarh 160030, India; prasenjit@csio.res.in

<sup>2</sup> Academy of Scientific and Innovative Research (AcSIR), Ghaziabad 201002, India

\* Correspondence: manoj.bhuyan@csio.res.in or manoj.femto@gmail.com

**Abstract:** The generation of optical beam arrays with prospective uses within the realms of microscopy, photonics, non-linear optics, and material processing often requires Dammann gratings. Here, we report the direct fabrication of one- and two-dimensional Dammann grating-like structures on soda lime glass using a nanosecond pulsed laser beam with a 1064 nm wavelength. Using the fabricated grating, an axicon lens, and an optical magnification system, we propose a scheme of generation of a diverging array of zero-order Bessel beams with a sub-micron-size central core, extending longitudinally over several hundred microns. Two different grating fabrication strategies are also proposed to control the number of Bessel beams in an array. It was demonstrated that Bessel beams of 12 degrees conical half-angle in an array of up to  $[5 \times 5]$  dimensions can be generated using a suitable combination of Dammann grating, axicon lens and focusing optics.

**Keywords:** laser fabrication; Dammann grating; material processing; Bessel beam array; optical imaging

## 1. Introduction

The optical beams in one-dimensional (1D) and two-dimensional (2D) array formats find numerous applications in emerging fields such as microscopy [1,2], photonics [3,4], nonlinear optics [5,6], optical trapping [7], beam shaping [8], laser fabrication [9,10], etc. For instance, Pushkarev et al. [6] have demonstrated arrays of nonlinear stable beams, often referred to as filament, using optical array generators such as phase plate and Dammann grating. Dammann grating is a phase grating that produces multiple light spots of equal intensity [11]. Such nonlinear arrayed beams are extremely useful for efficient THz generation and waveguiding [5] in a gas medium. Similarly, Zhu et al. [9] have demonstrated parallel fabrication capability using multifocal spots generated by a spatial light modulator (SLM) and a high numerical aperture (NA) objective lens. Ma et al. [3] have demonstrated matrix multiplications of 50 pairs of  $4 \times 8$  matrices using Dammann gratings involving digital micro-mirror arrays. The parallel multiphoton microscopy of microspheres and nanorods was also demonstrated by Gu et al. [1], wherein they generated  $[2 \times 2]$  multifocal arrays using an SLM. The importance of the applications mentioned above is further accelerated by the discovery of non-diffractive optical beams such as Bessel beams [12,13]. The remarkable properties of Bessel beams, such as their non-diffractive aspects, i.e., they resist diffraction, and self-healing, i.e., they recover the beam profile after encountering an obstacle, make the case for their being of prime importance in the fields of nonlinear optics, laser micro-fabrication, etc. [14,15]. Therefore, a range of novel applications may be envisaged by combining the concepts of optical beam array generation and non-diffractive beams with long propagation distances. A significant advancement has been made over the last decade towards realising Bessel beams in an array format.

García-Martínez et al. [16] have generated a two-dimensional array  $[4 \times 4]$  of diverging Bessel beams by applying Dammann grating and axicon lens phases with an SLM. In



**Citation:** Praharaj, P.; Bhuyan, M.K. Nanosecond Laser Fabrication of Dammann Grating-like Structure on Glass for Bessel-Beam Array Generation. *Photonics* **2024**, *11*, 473. <https://doi.org/10.3390/photonics11050473>

Received: 5 April 2024  
Revised: 11 May 2024  
Accepted: 14 May 2024  
Published: 18 May 2024



**Copyright:** © 2024 by the authors. Licensee MDPI, Basel, Switzerland. This article is an open access article distributed under the terms and conditions of the Creative Commons Attribution (CC BY) license (<https://creativecommons.org/licenses/by/4.0/>).

this case, the Bessel-beam array generation process can be understood as follows: the axicon lens produces single Bessel beam, which subsequently gets diffracted with multiple orders with the help of the Dammann grating. The phase  $g(r)$  of a classical linear axicon lens can be expressed as follows:  $g(r) = \exp\left(\frac{-2i\pi r}{r_0}\right)$ , where  $r = \sqrt{x^2 + y^2}$  is the radial coordinate and  $r_0$  is the parameter that defines the cone angle of Bessel beams. Values  $x$  and  $y$  are the Cartesian coordinates. The phase is further modified when axicon lens is associated with a one-dimensional grating of period  $P$ , which can be expressed as follows:  $g'(r) = \exp\left(\frac{-2i\pi r}{r_0}\right) \exp\left(\frac{2i\pi x}{P}\right)$ . This resulting phase  $g'(r)$  would eventually generate an array of Bessel beams [16]. Nevertheless, the diverging half-angle ( $\theta$ ) of multiple Bessel beams in the array can be calculated as follows:  $\theta = \sin^{-1}\left(\frac{n\lambda}{P}\right)$ , where  $n$  is the order of diffraction, and  $\lambda$  is the light wavelength. Lutz et al. [17] have generated a one-dimensional array [ $2 \times 1$ ] of 0.81-degree-diverging Bessel beams by applying the phase of a Dammann grating with an SLM combined with a 170-degree refractive axicon lens. Indeed, they have obtained arrayed zero-order Bessel beams of 7.6  $\mu\text{m}$  full width half maxima (FWHM) central core and successfully drilled 5  $\mu\text{m}$  diameter holes on aluminium foil using such beams. Using a spatial light modulator, Cheng et al. [18] have exploited the superposition of high-order Bessel beams to obtain tightly packed foci, retaining the non-diffractive length of 1 mm, and resembling an array of zero-order Bessel beams. Schwarz et al. [19] have generated an array of parallel zero-order Bessel beams using fused silica axicon lenslets in hexagonal arrangements by exploiting laser manufacturing techniques. In this case, 37 Bessel beams of FWHM central core sizes in the range of 9.4–10.3  $\mu\text{m}$  and FWHM non-diffractive lengths in the range of 8–8.5 mm were obtained by Schwarz et al. using an axicon lenslet array. Chen et al. [20] have generated Bessel-beam arrays [ $4 \times 4$ ] with a sub-wavelength size central core, i.e., 570 nm and non-diffractive length up to 60  $\mu\text{m}$ , using all-dielectric metasurfaces. In this case, the corresponding metasurfaces were created through the use of electron-beam lithography and lift-off processes. To summarise, Bessel beams in dense array format are typically generated by modulating the beam's phase at the pupil plane of a high-NA objective lens involving an SLM. However, the poor resolution of the spatial light modulator limits the phase discretisation and hence limits the generation of high-cone-angle Bessel beams. In contrast, a high-cone-angle Bessel beam array can be generated directly using metasurfaces, but the fabrication of such elements needs very high-end lithography techniques. Therefore, a simple method for generating a Bessel beam array is of prime importance and hence becomes the subject of the current study. Our study realised the described Bessel beam array using passive optical elements such as an axicon lens, laser-fabricated Dammann gratings, and an optical magnification system.

## 2. Experimental Design and Methods

The experimental setup employed for the grating fabrication is shown in Figure 1. The diode-pumped solid-state nanosecond pulsed laser source (Bright Solutions, Italy, Onda 1064 nm Model) emitted a radiation of wavelength 1064 nm, pulse durations in the range of 2–6 ns at a 100 kHz maximum rate of repetition, and 1 mJ of pulse energy. The laser beam was directed onto the samples (i.e., soda lime glass of 1 mm thickness) using an objective lens (Olympus Plan N 10X/0.25 NA). The glass samples were mounted on a motorized X(50 mm)-Y(50 mm)-Z(25 mm) translation stage assembly (Holmarc Opto-mechatronics Pvt. Ltd., India, MTS series). A delay generator (Lightigo s.r.o, Czech Republic, SyncRay Model) was employed to trigger both the laser source and translation stages; the pulse parameter selection and sample movement corresponding to a particular fabrication condition were controlled using a computer. To machine a Dammann grating on glass, the Gaussian laser focal point was adjusted with respect to the sample front surface by optimising the plasma intensity. Multiple pulse-based holes and single-pass-based trenches were machined on the sample surface prior to the Dammann grating fabrication experiments.

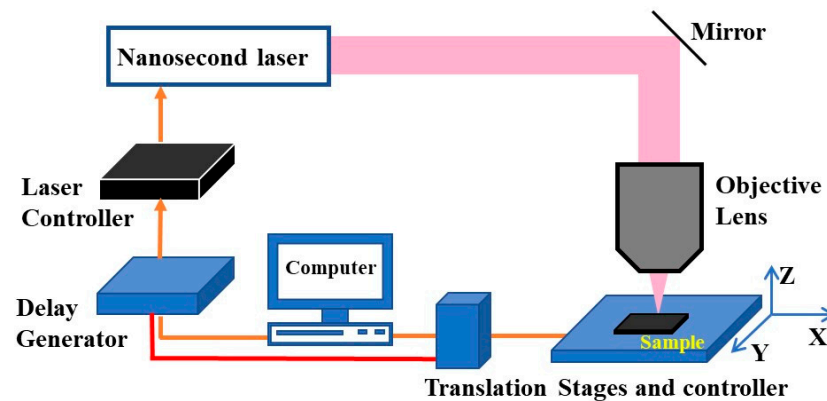


**Figure 1.** Schematic diagram of nanosecond pulsed laser micromachining setup.

For instance, single-pass trenches were machined on a glass surface using the following parameters: 5 kHz laser repetition rate, laser power in the range of 1–3.3 watts, scanning speed of 1.5 mm/s, and focal spot size ( $1/e^2$ ) of 14.6  $\mu\text{m}$ . The laser power was measured near the laser source. The morphological characteristics of machined features were then studied using optical microscopy (using Olympus’s CX33 Optical Microscope) and 3D Profilometry (using Bruker’s Contour GT-K 3D optical microscope) techniques. Figure 2a,b show the optical micrograph and 3D profile of trenches machined using laser fluence levels in the range of 191–789  $\text{J}/\text{cm}^2$ , respectively. Although material modification was evident for machining at a threshold fluence of 191  $\text{J}/\text{cm}^2$ , i.e., peak intensity of  $9.56 \times 10^{10} \text{ W}/\text{cm}^2$ , the machining condition could not produce continuous line structures on glass. Nevertheless, the variation of trench width obtained from the optical micrograph with respect to the laser fluence is shown in Figure 2c; the trench width evolves near-linearly (except for the threshold fluence), with increasing laser fluence levels. It was also observed that the trench depth nearly saturates at 40  $\mu\text{m}$  when machined using laser fluence in the range of 239–789  $\text{J}/\text{cm}^2$ . The trench machining strategy was eventually followed to realise large machined areas, which are an integral part of grating. In this case, the inter-line spacing, i.e., pitch, was maintained at 10  $\mu\text{m}$ . The binary phase Dammann gratings were fabricated on glass to generate multiple orders of diffraction based on the number and position of transition points, i.e., the  $0-\pi$  phase change point of the grating. Here, we have adopted the transition points determined through the cost function optimisation method by Zhou et al. [21]. The transition point of grating for a one-dimensional (1D) two-spot ( $1 \times 2$ ) array is [0.5]. Similarly, the transition points for the five-spot ( $1 \times 5$ ) array are [0.03863, 0.39084, 0.65552]. In the case of two-dimensional (2D) beam array generation, the above transition points can be extended in a plane. In this study, we have fabricated gratings to generate both 1D and 2D arrays of optical Bessel beams.

The Bessel beam generation and characterisation setups were developed to evaluate the performance of fabricated gratings, as shown in Figure 3a and b, respectively. The Gaussian CW laser beams of 532 nm wavelength were first expanded and incident on the fabricated grating, followed by a polymer linear-phase axicon lens of a 177-degree apex angle. This grating–axicon combination generates an array of zero-order Bessel beams. The generated Bessel beam array was further de-magnified using a telescopic arrangement involving a plano-convex lens ( $f = 150 \text{ mm}$ ) and an objective lens of 20X/0.4 NA to obtain a micro-Bessel beam array. To characterise the generated micro-Bessel beam array, an imaging setup (see Figure 3b) comprising a CMOS camera in combination with a set of lenses (a plano-convex lens ( $f = 150 \text{ mm}$ ) and an objective lens of 20X/0.4 NA), resulting in a magnification of 32, was developed. A series of transverse Bessel beam profiles at every 5 microns along the beam propagation direction was recorded (using 0.5 ms camera exposure time) for further image processing. Note that in the absence of grating, the present setup generates single micro-Bessel beams. Figure 3c,d show the typical longitudinal and radial cross-sectional profiles of Bessel beams of conical half-angles of 12 degrees generated

in the experiment. In this case, the Bessel beam central core size (FWHM) and longitudinal extent (FWHM) were measured at 0.9  $\mu\text{m}$  and 220  $\mu\text{m}$ , respectively.

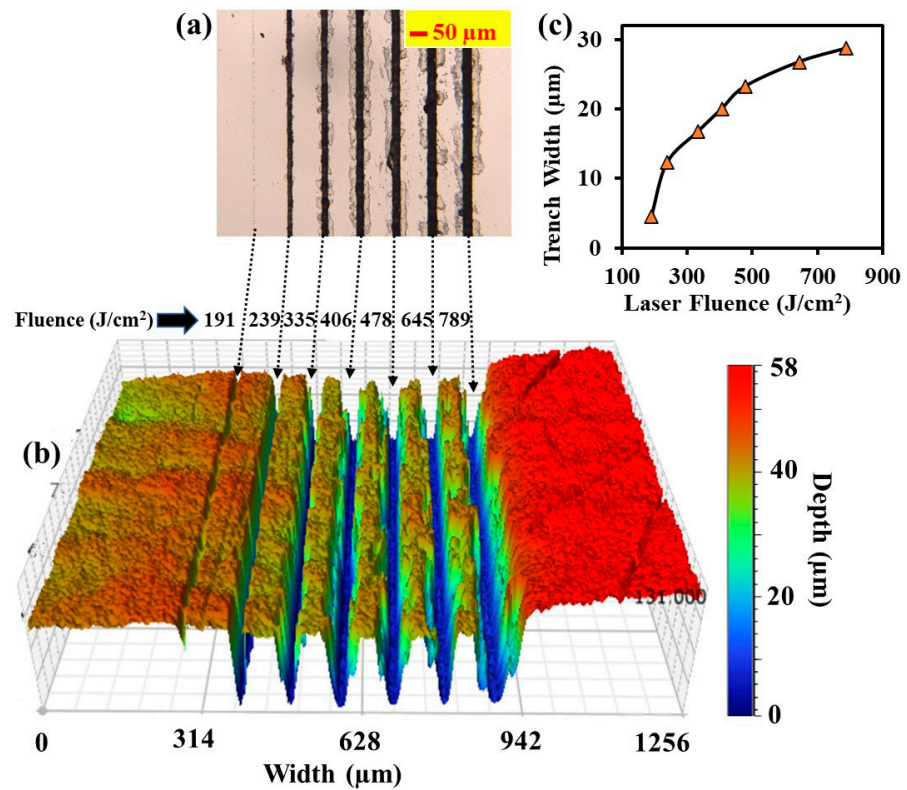
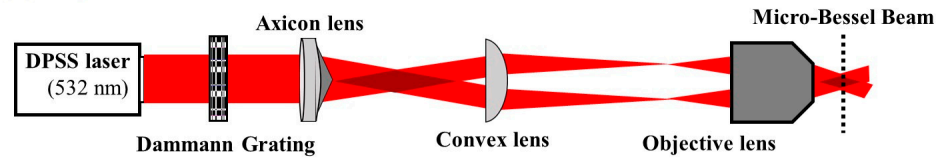


**Figure 2.** (a) Optical micrograph of trenches machined (on a single-pass basis) on the front surface of glass using nanosecond laser pulses of the following fluence levels: 191, 239, 335, 406, 478, 645 and 789  $\text{J}/\text{cm}^2$ . (b) As described above, 3D profilometric images of trenches. (c) Plot showing the variation of trench width with respect to laser fluence.

**(a) Setup 1: Bessel Beam Generation**



**(b) Setup 2: Bessel Beam Characterisation**

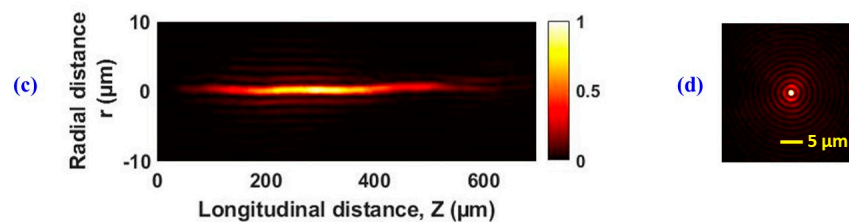
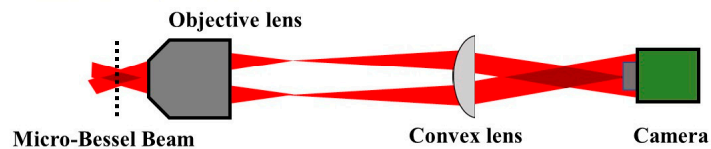


**Figure 3.** Schematics of Bessel beam generation and characterisation setups are shown in (a,b), respectively. (c) Cross-sectional profile image of generated Bessel beams of 12-degree conical half-angle. (d) Typical radial profile of generated Bessel beams showing concentric rings.

### 3. Experimental Results

The experimental results in connection with the fabricated one-dimensional (1D) gratings and the respective Bessel beam arrays are shown in Figure 4. For every grating, we define the following parameters: Transparent zone (TZ) is defined as the portion of the width of the material which is not machined. The opaque zone (OZ) is defined as the width of the laser-machined trench on the surface of a material. Period (P) is defined as the sum of TZ and OZ. For instance, a few 1D gratings were machined using a laser fluence of  $335 \text{ J/cm}^2$ , with fixed  $P = 200 \text{ }\mu\text{m}$ , but with varying TZs and OZs; the corresponding optical micrographs and 3D profiles are shown as insets of Figure 4a–c. The depth profile, in particular that of the grating of  $\text{TZ} = 100 \text{ }\mu\text{m}$ ,  $\text{OZ} = 100 \text{ }\mu\text{m}$ , follows a U-shape. The depth of the gratings, as measured from 3D profile images, was approximately  $40 \text{ }\mu\text{m}$ . When such gratings were employed for Bessel beam array generation, it was observed that the number of Bessel beams increased from 3 to 7 by increasing the OZ from 20 to  $100 \text{ }\mu\text{m}$  of the grating. In contrast, the normal transmission of the gratings was decreased from 67 to 43% (with a measurement error of up to 2%) by increasing the OZ from 20 to  $100 \text{ }\mu\text{m}$ . It was also observed that the overall characteristics of the original isolated Bessel beam, i.e., one generated using the axicon alone, remain preserved in the array format. However, the Bessel beam longitudinal, i.e., axial, intensity is modulated with the increasing opaque-zone length of the grating. For instance, in the case of grating of  $\text{TZ} = 100 \text{ }\mu\text{m}$ ,  $\text{OZ} = 100 \text{ }\mu\text{m}$ , the average Bessel beam axial modulation distance was measured to be approximately  $90 \text{ }\mu\text{m}$ . This axial modulation can be attributed to the non-uniformity of laser-machined patches of grating. Also, we cannot rule out the Talbot effect, i.e., axial intensity modulation [22,23] which normally appears when light passes through a grating-like structure. In the present case, the Talbot distance ( $= 2P^2/\lambda$ ) was calculated to be  $540 \text{ }\mu\text{m}$ . Therefore, the axial modulation can be due to a fractional Talbot effect, although this needs to be verified through experiments.

1D gratings were also fabricated by varying the laser fluence levels, keeping the grating parameter fixed at  $\text{TZ} = \text{OZ} = 100 \text{ }\mu\text{m}$ . Figure 4d–f depict the longitudinal cross-section images of Bessel beam arrays generated using gratings fabricated with laser fluence levels of 335, 478, and  $645 \text{ J/cm}^2$ , respectively. It is apparent from the figure that the number of Bessel beams in the array only increases from 7 to 9 by increasing the laser power for grating fabrication. However, the normal transmission of the gratings was severely decreased, changing from 46 to 23% (with a measurement error of up to 2%) with an increase in the laser fluence level for grating fabrication from 335 to  $645 \text{ J/cm}^2$ . The quality of the Bessel beam array in terms of uniformity is also poor when the gratings are machined with high laser power. In an attempt to enhance the transmission of the grating, etching (using 5% HF + 95% water solution, and 40 min of etching time) was performed on the fabricated grating. Indeed, the grating transmission was enhanced from 46% to 49%, 32% to 51%, and 23% to 43%, corresponding to the laser fluence levels of 335, 478, and  $645 \text{ J/cm}^2$ , respectively, as used for grating fabrication.

To study the influence of the “periods” of the gratings on the Bessel beam array generation, 1D gratings were fabricated, using a fixed laser fluence of  $335 \text{ J/cm}^2$ , with different grating periods. In all of the cases considered, the laser-machined trench width is half of the grating period size, i.e.,  $\text{TZ} = \text{OZ} = P/2$ . Figure 5a–d show the longitudinal cross-section images of Bessel beam arrays generated using the fabricated gratings with the following periods (P): 120, 200, 400 and  $800 \text{ }\mu\text{m}$ , respectively. It is apparent from the figure that the number of Bessel beams, along with their longitudinal extent in the array, decreases from 7 to 3 with an increase in the grating period size from 120 to  $800 \text{ }\mu\text{m}$ . It was also observed that the diverging half-angles such as  $\theta_1$  (first-order),  $\theta_2$  (second-order), and  $\theta_3$  (third-order) of the Bessel beams vary with respect to the period of the gratings involved; diverging half-angles decrease with increased grating period. For instance, the diverging half-angles of the Bessel beam array generated using a  $200 \text{ }\mu\text{m}$  period grating (see Figure 5b) are as follows:  $\theta_1 = 2.2^\circ$ ,  $\theta_2 = 4.5^\circ$ , and  $\theta_3 = 6.7^\circ$ . Interestingly, the diverging half-angle of the Bessel beam array, generated using an  $800 \text{ }\mu\text{m}$  period grating (see Figure 5d), is

sufficiently low, i.e.,  $0.4^\circ$ . However, in this instance, an evolutionary phase of Bessel beams, extended over a considerable range, and spanning a few hundred microns was observed.

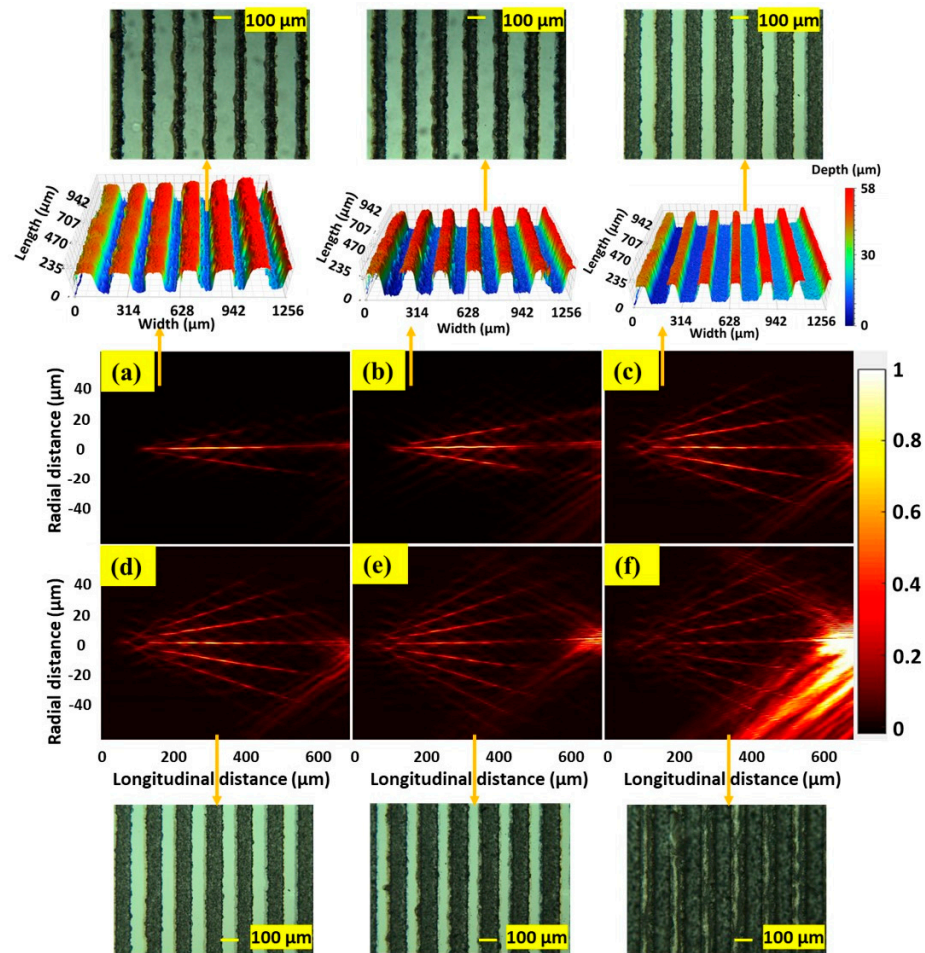


**Figure 4.** Cross-sectional images of zero-order Bessel beams in an array format. Bessel beams in array format were generated using axicon lens, telescope and different Dammann gratings (machined with a laser fluence of  $335 \text{ J/cm}^2$ ) of fixed period ( $P$ ) of  $200 \mu\text{m}$ , with various combinations of transparent zone (TZ) and opaque zone (OZ): (a) TZ =  $180 \mu\text{m}$ , OZ =  $20 \mu\text{m}$ ; (b) TZ =  $150 \mu\text{m}$ , OZ =  $50 \mu\text{m}$ ; and (c) TZ =  $100 \mu\text{m}$ , OZ =  $100 \mu\text{m}$ . Bessel beam arrays were also generated using Dammann gratings of defined parameters, i.e., TZ = OZ =  $100 \mu\text{m}$ , which were machined with various laser fluence levels: (d)  $335 \text{ J/cm}^2$ , (e)  $478 \text{ J/cm}^2$ , and (f)  $645 \text{ J/cm}^2$ . The insets show the optical micrographs and 3D profiles of Dammann gratings in each case.

For better illustration, Bessel beam array generation using fabricated gratings with periods of  $200 \mu\text{m}$  and  $800 \mu\text{m}$  were given emphasis. In such cases, the transverse profiles of the Bessel beam arrays at different longitudinal distances, i.e.,  $Z_1 = 120 \mu\text{m}$ ,  $Z_2 = 240 \mu\text{m}$ , and  $Z_3 = 430 \mu\text{m}$ , are shown in Figure 5e–j. It is evident from the figure and insets that the strength of individual Bessel beams in the array varies from one to the other, i.e., there is maximum intensity in the zero-order and then gradually diminished intensities in the high-order. The occurrence of non-uniform beam strengths in the array may be due to the suboptimal grating depth profiles [10,24]. From a quantitative viewpoint, the radial distances between individual Bessel beams of an array with respect to the central Bessel beams were calculated considering the light wavelength,  $\lambda = 532 \text{ nm}$ . Figure 5k displays the tabulated values corresponding to respective gratings with periods of  $200 \mu\text{m}$  and  $800 \mu\text{m}$ . In case of the  $200 \mu\text{m}$  period grating, it was observed that the three well-separated Bessel beams appear only beyond a longitudinal distance of  $200 \mu\text{m}$ . The radial profile of Bessel beam arrays corresponding to a representative case, i.e.,  $Z_2 = 240 \mu\text{m}$ , is shown in Figure 5f,

wherein the zero-order and first-order Bessel beams are separated by a radial distance of  $17 \lambda$ . Prior to this longitudinal distance, overlapping of adjacent Bessel rings occurs, as evident from Figure 5e. Such features were earlier observed for both zero-order and high-order Bessel beams [25,26]; the authors observed that the complete radial separation between adjacent Bessel beams depends on the longitudinal distance of Bessel beams. Contrastingly, in case of the  $800 \mu\text{m}$  period grating, it was observed that the three well-separated Bessel beams appear only beyond a longitudinal distance of  $400 \mu\text{m}$ . Figure 5l shows the decreasing trend of diverging half-angles of Bessel beams (only first-order) in an array with respect to the increasing grating period. Indeed, a Bessel beam array [ $1 \times 3$ ] of a diverging half-angle of 6 degrees was successfully generated using laser-fabricated gratings with a period of  $80 \mu\text{m}$ .

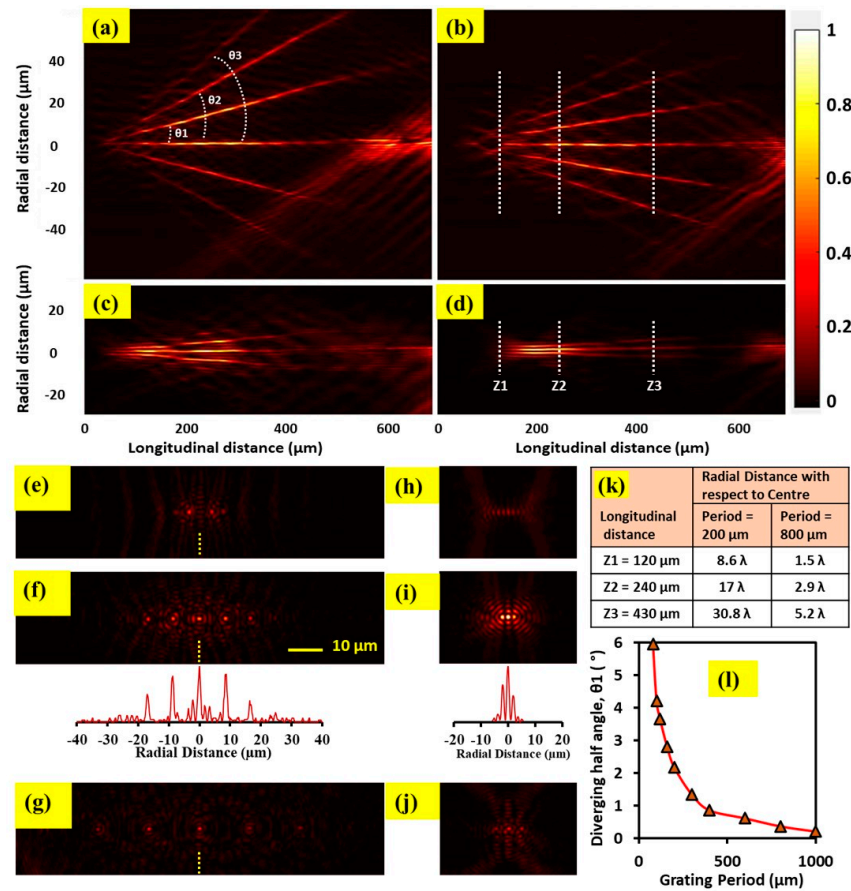


**Figure 5.** Cross-sectional images of arrayed Bessel beams generated using an axicon lens, telescope, and Dammmann gratings (machined with a laser fluence of  $335 \text{ J}/\text{cm}^2$ ) of the following parameters: (a)  $\text{TZ} = \text{OZ} = 60 \mu\text{m}$ , (b)  $\text{TZ} = \text{OZ} = 100 \mu\text{m}$ , (c)  $\text{TZ} = \text{OZ} = 200 \mu\text{m}$ , and (d)  $\text{TZ} = \text{OZ} = 400 \mu\text{m}$ . (e–j) Also shown here are the radial profiles of the Bessel beam array captured at three longitudinal distances, i.e.,  $Z = 120 \mu\text{m}$ ,  $240 \mu\text{m}$  and  $430 \mu\text{m}$ , respectively, corresponding to the cases (b,d). These longitudinal positions are marked as Z1, Z2, and Z3 on the images. The radial intensity profiles corresponding to images (f,i) are insets. (k) A table indicating the inter-Bessel beam separation (with respect to the central Bessel beam) at longitudinal distances of  $120 \mu\text{m}$ ,  $240 \mu\text{m}$ , and  $430 \mu\text{m}$ , as associated with two distinct gratings. (l) Plot showing the variation of diverging half-angle  $\theta_1$  of Bessel beam arrays as a function of the grating period.

The idea of Bessel beam array generation using laser-fabricated Dammmann grating was also extended to 2D. To do so, two different grating fabrication strategies were developed. In the first case, transparent zones and opaque zones, i.e., laser-machined (using laser fluence of  $335 \text{ J}/\text{cm}^2$ ) zones of nearly  $100 \mu\text{m}$  each (corresponding to the grating period of  $200 \mu\text{m}$ ), were first fabricated in one axis, and the same patterns were created in the

perpendicular axis of the same plane. Here, we refer to the machining strategy as the “line-scanning” strategy, as the laser continuously machines the sample surface along a line. As a result, square-size transparent zones were created at the corners in a square lattice, as shown in Figure 6a. In the second case, laser machining was performed with another machining strategy, referred to as the “patch-scanning” strategy. In this case, the machining was performed in patches (corresponding to the grating period of 200 μm) at selective locations on the sample surface. As a result, square-sized transparent zones were created at the corners and the centre in a square lattice, as shown in Figure 6b. The 3D profiles of both considered gratings are also shown as insets to Figure 6. When such gratings were employed for generating a Bessel beam array in two dimensions, the Bessel beam configuration appeared to be very contrasting. Figure 6c,d show the typical transverse profiles at a near-longitudinal-intensity maximum position of a Bessel beam (FWHM core size of 0.9 μm) array generated using gratings fabricated with line-scanning and patch-scanning strategies, respectively. It is apparent from the figures that a denser array of Bessel beams can be generated using gratings fabricated with the line-scanning strategy.

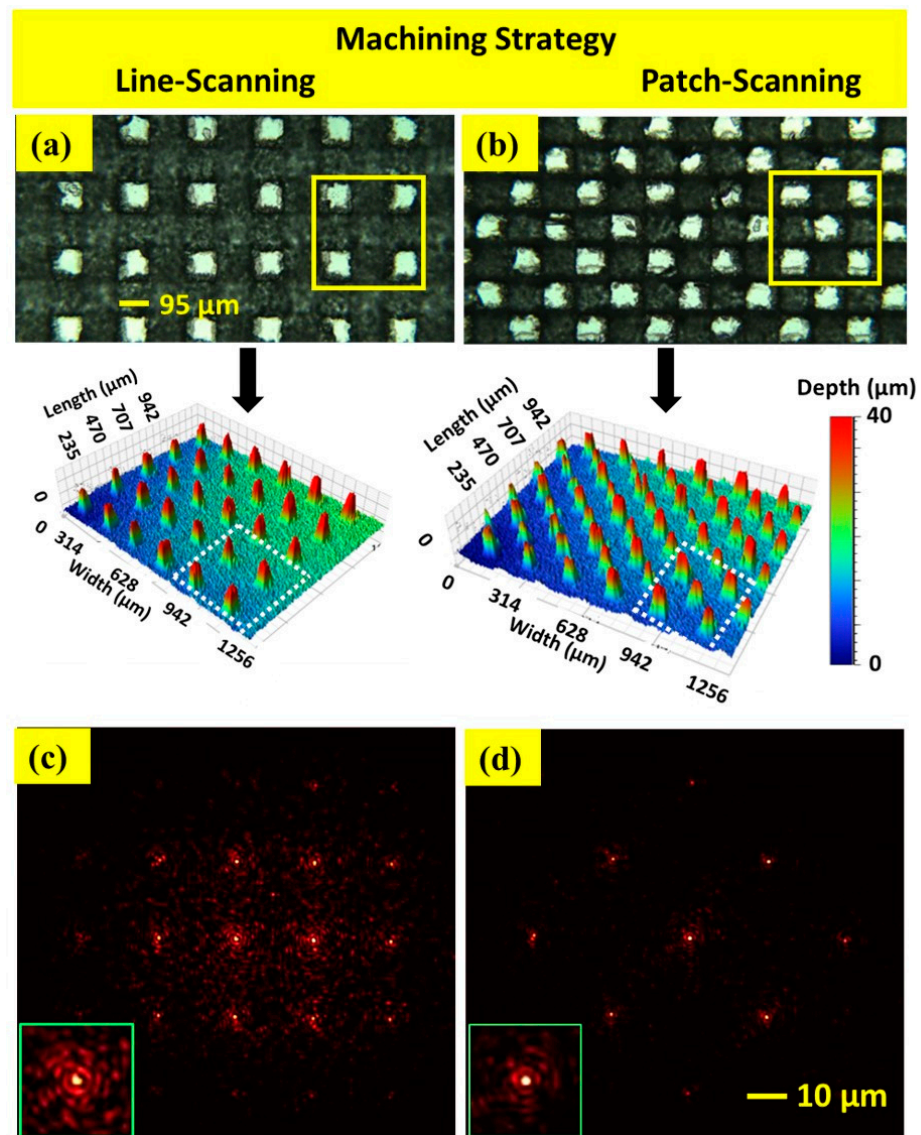


**Figure 6.** Optical micrographs of 2D Dammann gratings with periods of 200 μm fabricated using a laser fluence of 335 J/cm<sup>2</sup> with (a) line-scanning and (b) patch-scanning strategies. The corresponding

3D profiles of gratings are shown as insets. (c,d) The typical radial profiles of 2D Bessel beam arrays are generated using an axicon lens and gratings machined with both considered scanning strategies. The insets to (c,d) show the enlarged size of Bessel beams placed at the centre of the array.

To generate Bessel beams of the desired array configuration, the grating transition points need to be fixed. For instance, the transition points corresponding to a five-spot  $[1 \times 5]$  array are  $[0.03863, 0.39084, 0.65552]$ . In such cases, the opaque zones, i.e., laser-machined zones, were obtained on glass according to the transition points in a 1D plane. Figure 7a shows the microscopic image of a 1D Dammann grating with non-uniform transparent zone spacing. In this case, when the fabricated 1D grating was employed for array generation, a  $[1 \times 5]$  Bessel beam array was obtained; Figure 7b–d show the transverse profiles of the Bessel beam array at  $Z = 190 \mu\text{m}$ ,  $295 \mu\text{m}$ , and  $335 \mu\text{m}$ , respectively. It was observed that the well-separated Bessel beams in the array appear beyond the longitudinal distance of  $330 \mu\text{m}$ . Figure 7b,c show the radial profiles of Bessel beam array corresponding to the evolutionary phases of Bessel beams.

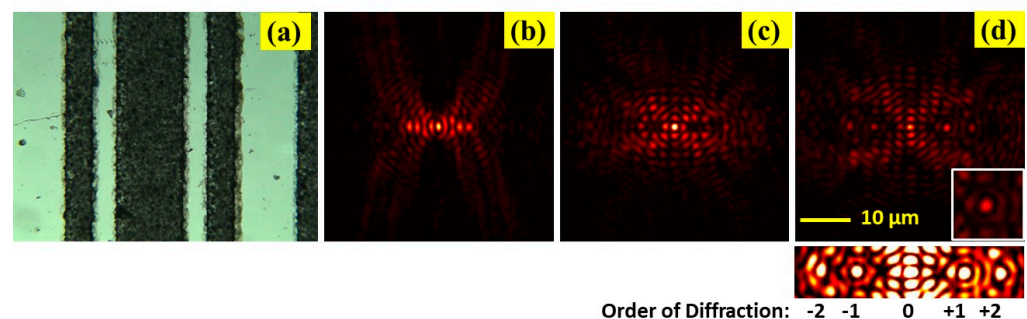


**Figure 7.** (a) Optical micrograph of laser fabricated (using laser fluence of  $335 \text{ J/cm}^2$ ) 1D Dammann grating for the generation of a  $[1 \times 5]$  Bessel beam array. (b–d) Also shown here are the radial profiles of the Bessel beam array captured at three longitudinal distances, i.e.,  $Z = 190 \mu\text{m}$ ,  $295 \mu\text{m}$ , and  $335 \mu\text{m}$ , respectively. The inset to (d) shows the central portion of the corresponding saturated image.

#### 4. Discussion

Diffractive optical elements such as Dammann gratings are crucial components for generating optical beam arrays. Therefore, the key findings of the present study relate to the fabrication of Dammann-like gratings on glass surfaces and their respective roles in forming the Bessel beam array. In general, the phase profile of Dammann grating is governed by controlled depth patterns on a transparent dielectric material. From the fabrication viewpoint, reactive ion etching is the prevailing method, but obtaining a controlled depth on glass using this method is difficult. The state-of-the-art in this fabrication domain incorporates electron-beam pattern generators with nanometre-fabrication resolution. However, the adoption of such an instrument is limited by instrument cost and stringent machining conditions. In this respect, the laser machining technique offers a versatile solution. For instance, multifocal spot arrays up to  $[5 \times 5]$  were realised using 2D Dammann gratings on sapphire plates machined using  $400 \text{ nm}$  wavelength femtosecond laser beams and wet etching [27]. In contrast, we offer an economic Dammann grating machining method using nanosecond laser beams as demonstrated in the current investigation.

One of the interesting features of our Bessel beam array generation scheme is that it does not require Dammann grating of critical sub-micron depth profiles to obtain an array of zero-order Bessel beams with a sub-micron-size central core. Instead, Dammann gratings with periods in the range of hundreds of microns and depths in the range of tens of microns may be employed in combination with an axicon lens and an optical magnification system comprising a high-NA objective lens to generate a Bessel beam array (see Figure 2). There are several advantages associated with our developed Bessel beam array generation methodology. (1) A high-NA objective lens ensures small core-size, i.e., high cone-angle Bessel beams [28]. (2) The onset position of beam array lies at the focal point of the

objective lens; this condition is advantageous for parallel micromachining and microscopy applications. For sake of comparison, when phase coded Dammann grating is employed to directly realize a Bessel beam array, the onset point lies right next to the grating, putting limitations on the above-mentioned applications. (3) Both Bessel beam characteristics and their array format can be controlled independently by choice of the axicon lens and grating, respectively. In contrast, a Dammann grating multiplexed with axicon phase can generate only a single type and configuration of Bessel beam array. Of course, a SLM-based Bessel beam array generation method can offer flexibility in getting the desired Bessel beam (low cone angle Bessel beams only) characteristics and their array format. However, because of the typically low laser-damage threshold of the SLM, such a scheme cannot be implemented for high-power applications such as those in plasma physics.

Gratings on glass were fabricated using standard machining techniques involving a few kHz repetition rate nanosecond pulsed laser beams [29]. Grating periods were maintained by single-pass laser scanning across the sample surface. For the sake of consistency, we choose a laser fluence of  $335 \text{ J/cm}^2$  for the fabrication of uniform grating structures. It is obvious that the laser machining would result in plenty of debris, hindering the grating transmittance. Therefore, prior to the application, gratings were rinsed with water after machining. Further etching of the grating additionally increased transmission, which reached a peak value of approximately 50%. This enhancement occurs because the half-period region becomes opaque as a result of the laser machining.

From the Bessel beam array generation capability viewpoint, the grating period plays a key role. For instance, by keeping the period same, one can vary the number of Bessel beams in an array by employing gratings of increased opaque-zone widths (see Figure 4a–c). Grating depth seems not to be critical in deciding the number of Bessel beams in an array (see Figure 4d–f). Indeed,  $[1 \times 9]$  arrayed zero-order Bessel beams were produced using grating with a period  $200 \mu\text{m}$  with a transition point of 0.5. Ideally, a grating of the transition point of 0.5 should generate an array of  $[1 \times 2]$ , as calculated by Zhou et al. [21], with the condition that the grating depth is maintained to create  $\pi$ -phase shift. For example, for an incident light of  $532 \text{ nm}$  wavelength ( $\lambda$ ) and glass refractive index ( $n$ ) of 1.51, the ideal grating depth ( $d$ ) corresponding to a phase delay ( $\vartheta$ ) of  $\pi$  can be estimated as follows:  $d = [\vartheta/\pi][\lambda/2(n - 1)] = 522 \text{ nm}$ . Indeed, earlier reports suggest that zero-order diffraction becomes prominent if the grating depth does not match the estimated one [10,24]. Since our grating depths were in the order of tens of microns, we excited not only zero-order diffraction but also high-order diffraction. We also observe that the spatial characteristics of zero-order Bessel beams in isolated form (i.e., those generated using only the axicon lens) remain preserved in the case of an array format (i.e., when generated using both an axicon lens and Dammann grating). The FWHM central core and non-diffracting length of zero-order Bessel beams in both isolated and array formats were  $0.9 \mu\text{m}$  and  $220 \mu\text{m}$ , respectively. There are several beam-array configurations reported in the literature [17–20]. The present study deals with the generation of diverging Bessel beam array configurations. It has been observed that the diverging angle of the Bessel beam array decreases with an increase in the grating period, as evident from Figure 5a–d. For example, the diverging half-angle of the first-order Bessel beam in the array generated by grating of a period of  $120 \mu\text{m}$  was measured to be 3.7 degrees, which corresponds to  $\text{NA} = 0.1$ . Similarly, the diverging half-angle of the third-order Bessel beam in the array was measured to be 11 degrees, which corresponds to  $\text{NA} = 0.29$ . In contrast, when grating of a period of  $800 \mu\text{m}$  was employed, the diverging half-angle of the first-order Bessel beam (other orders are barely visible) in the array was measured at 0.4 degrees, quite analogous to a parallel Bessel beam array.

The above machining approach can be easily extended over two-dimensional space to obtain a 2D Dammann grating. Two primary laser machining approaches, i.e., line-scanning and patch-scanning, were explored. In the case of line scanning, the laser beam traverses first one axis, followed by the other axis, resulting in a unit cell consisting of four square pieces with transparent zones at the corners. In contrast, in the case of patch-scanning,

laser machines glass surface in such a way that a unit cell consisting of four square pieces with transparent zones at the corners as well as in the centre forms. Interestingly, different configurations of the Bessel beam array were obtained when the 2D gratings used were machined with different strategies (see Figure 6); a denser array can be obtained with grating machined using line-scanning strategy. An ideal 1D Dammann grating with unique transition points [21] was thus obtained using the line-scanning machining strategy; a  $[1 \times 5]$  array of zero-order Bessel beams was obtained using suitable gratings (see Figure 7). We, therefore, anticipate here that the developed grating fabrication strategy involving an economic nanosecond-laser-pulse-based machining setup would be highly useful in the realisation of array of different classes of non-diffractive optical beams, with potential applications in emerging areas such as microscopy, nonlinear optics, and micro- and nanofabrication. As perspective for future work, various aspects of the Bessel beam array may be studied. For instance, controlling the axial intensity [30] and polarization states [31] of individual Bessel beams given an array of arbitrary configuration would be useful for the above-mentioned applications.

## 5. Conclusions

One- and two-dimensional Dammann grating-like structures were successfully fabricated on soda lime glass using a nanosecond pulsed laser machining technique, and their transmission and beam array generation capability were identified. Gratings with a period in the range of 80–1000 microns were machined on the upward-facing surfaces of glass materials. Zero-order Bessel beams of conical half-angles up to 12 degrees in 1D and 2D array format were successfully generated involving the fabricated gratings, an axicon lens, and an optical magnification system. The number of Bessel beams in a diverging array, i.e., with a maximum value of 9, and their configuration, i.e., beamlet position, were controlled by choosing the laser fabrication strategy, either line- or patch-scanning, and defining a grating period. We, therefore, anticipate that the demonstrated grating fabrication techniques and scheme of Bessel beam array generation will have direct implications in the fields of parallel material processing, microscopy, non-linear optics, beam shaping, and plasma physics.

**Author Contributions:** Conceptualization and methodology, P.P. and M.K.B.; experiments, P.P. and M.K.B.; data analysis, P.P. and M.K.B.; writing—original draft preparation, P.P.; writing—review and editing, P.P. and M.K.B.; supervision, M.K.B. project administration and funding acquisition, M.K.B. The authors declare that no AI support was used. All authors have read and agreed to the published version of the manuscript.

**Funding:** This research was funded by DST-SERB, grant number SRG/2020/001538.

**Institutional Review Board Statement:** Not applicable.

**Informed Consent Statement:** Not applicable.

**Data Availability Statement:** The experimental data used to support the findings of this study are available from the corresponding author upon reasonable request.

**Acknowledgments:** The authors acknowledge Manoj Kumar Patel (CSIR-CSIO, Chandigarh) for providing Olympus's CX33 Optical Microscope and Bruker's Contour GT-K 3D optical microscope. The authors acknowledge Vinod Mishra (CSIR-CSIO, Chandigarh) for providing the polymer axicon.

**Conflicts of Interest:** The authors declare no conflicts of interest.

## References

1. Gu, M.; Lin, H.; Li, X. Parallel Multiphoton Microscopy with Cylindrically Polarized Multifocal Arrays. *Opt. Lett.* **2013**, *38*, 3627–3630. [[CrossRef](#)]
2. Ma, Q.; Khademhosseini, B.; Huang, E.; Qian, H.; Bakowski, M.A.; Troemel, E.R.; Liu, Z. Three-Dimensional Fluorescent Microscopy via Simultaneous Illumination and Detection at Multiple Planes. *Sci. Rep.* **2016**, *6*, 31445. [[CrossRef](#)]
3. Ma, G.; Yu, J.; Zhu, R.; Zheng, F.; Zhou, C.; Situ, G. Dammann Gratings-Based Truly Parallel Optical Matrix Multiplication Accelerator. *Opt. Lett.* **2023**, *48*, 2301–2304. [[CrossRef](#)]

4. Morrison, R.L.; Walker, S.L.; Cloonan, T.J. Beam Array Generation and Holographic Interconnections in a Free-Space Optical Switching Network. *Appl. Opt.* **1993**, *32*, 2512. [[CrossRef](#)] [[PubMed](#)]
5. Panov, N.; Andreeva, V.; Kosareva, O.; Shkurinov, A.; Makarov, V.A.; Bergé, L.; Chin, S.L. Directionality of Terahertz Radiation Emitted from an Array of Femtosecond Filaments in Gases. *Laser Phys. Lett.* **2014**, *11*, 125401. [[CrossRef](#)]
6. Pushkarev, D.V.; Lar'kin, A.S.; Mitina, E.V.; Zhidovtsev, N.A.; Uryupina, D.S.; Volkov, R.V.; Karpeev, S.V.; Khonina, S.N.; Karabutov, A.A.; Geints, Y.E.; et al. Robust Multifilament Arrays in Air by Dammann Grating. *Opt. Express* **2021**, *29*, 34189–34204. [[CrossRef](#)]
7. Ji, X.; Xu, S.; Gu, S. Generation of Atomic Optical Lattices by Dammann Gratings. *Adv. Opt. Technol.* **2012**, *2012*, 647657. [[CrossRef](#)]
8. Jahns, J.; Downs, M.M.; Prise, M.E.; Streibi, N.; Walker, S.J. Dammann Gratings For Laser Beam Shaping. *Opt. Eng.* **1989**, *28*, 281267. [[CrossRef](#)]
9. Zhu, Y.; Zhang, C.; Gong, Y.; Zhao, W.; Bai, J.; Wang, K. Realization of Flexible and Parallel Laser Direct Writing by Multifocal Spot Modulation. *Opt. Express* **2021**, *29*, 8698–8709. [[CrossRef](#)]
10. Kuang, Z.; Perrie, W.; Liu, D.; Edwardson, S.P.; Jiang, Y.; Fearon, E.; Watkins, K.G.; Dearden, G. Ultrafast Laser Parallel Microprocessing Using High Uniformity Binary Dammann Grating Generated Beam Array. *Appl. Surf. Sci.* **2013**, *273*, 101–106. [[CrossRef](#)]
11. Dammann, H.; Görtler, K. High-Efficiency in-Line Multiple Imaging by Means of Multiple Phase Holograms. *Opt. Commun.* **1971**, *3*, 312–315. [[CrossRef](#)]
12. Durnin, J.; Miceli, J.; Eberly, J.H. Diffraction-Free Beams. *Phys. Rev. Lett.* **1987**, *58*, 1499–1501. [[CrossRef](#)] [[PubMed](#)]
13. Mcgloin, D.; Dholakia, K. Bessel Beams: Diffraction in a New Light. *Contemp. Phys.* **2005**, *46*, 15–28. [[CrossRef](#)]
14. Bhuyan, M.K.; Sugioka, K. Ultrafast Laser Micro and Nano Processing of Transparent Materials—From Fundamentals to Applications. In *Advances in the Application of Lasers in Materials Science*; Ossi, P.M., Ed.; Springer International Publishing: Cham, Switzerland, 2018; Volume 274, pp. 149–190. ISBN 978-3-319-96845-2.
15. Marcinkevičius, A.; Marcinkevičius, M.; Juodkazis, S.; Matsuo, S.; Mizeikis, V.; Misawa, H. Application of Bessel Beams for Microfabrication of Dielectrics by Femtosecond Laser. *Jpn. J. Appl. Phys.* **2001**, *40*, L1197. [[CrossRef](#)]
16. García-Martínez, P.; Sánchez-López, M.M.; Davis, J.A.; Cottrell, D.M.; Sand, D.; Moreno, I. Generation of Bessel Beam Arrays through Dammann Gratings. *Appl. Opt.* **2012**, *51*, 1375–1381. [[CrossRef](#)] [[PubMed](#)]
17. Lutz, C.; Schwarz, S.; Marx, J.; Esen, C.; Hellmann, R. Multi-Bessel Beams Generated by an Axicon and a Spatial Light Modulator for Drilling Applications. *Photonics* **2023**, *10*, 413. [[CrossRef](#)]
18. Cheng, H.; Xia, C.; Kuebler, S.M.; Golvari, P.; Sun, M.; Zhang, M.; Yu, X. Generation of Bessel beam Arrays for Parallel Fabrication in Two-Photon Polymerization. *J. Laser Appl.* **2021**, *33*, 012040. [[CrossRef](#)]
19. Schwarz, S.; Rung, S.; Esen, C.; Hellmann, R. Rapid Fabrication of Precise Glass Axicon Arrays by an All Laser-Based Manufacturing Technology. *J. Laser Appl.* **2020**, *32*, 012001. [[CrossRef](#)]
20. Chen, L.; Kanwal, S.; Yu, B.; Feng, J.; Tao, C.; Wen, J.; Zhang, D. Generation of High-Uniformity and High-Resolution Bessel Beam Arrays through All-Dielectric Metasurfaces. *Nanophotonics* **2022**, *11*, 967–977. [[CrossRef](#)]
21. Zhou, C.; Liu, L. Numerical Study of Dammann Array Illuminators. *Appl. Opt.* **1995**, *34*, 5961–5969. [[CrossRef](#)]
22. Talbot, H.F. LXXVI. Facts Relating to Optical Science. No. IV. *Lond. Edinb. Dublin Philos. Mag. J. Sci.* **1836**, *9*, 401–407. [[CrossRef](#)]
23. Rayleigh, L. XXV. On Copying Diffraction-Gratings, and on Some Phenomena Connected Therewith. *Lond. Edinb. Dublin Philos. Mag. J. Sci.* **1881**, *11*, 196–205. [[CrossRef](#)]
24. Pang, H.; Cao, A.; Liu, W.; Shi, L.; Deng, Q. Alternative Design of Dammann Grating for Beam Splitting With Adjustable Zero-Order Light Intensity. *IEEE Photonics J.* **2019**, *11*, 1500909. [[CrossRef](#)]
25. Orlov, S.; Juršenas, A.; Baltrukonis, J.; Jukna, V. Controllable Spatial Array of Bessel-like Beams with Independent Axial Intensity Distributions for Laser Microprocessing. *J. Laser Micro Nanoeng.* **2018**, *13*, 324–329. [[CrossRef](#)]
26. Šlevas, P.; Orlov, S. Creating an Array of Parallel Vortical Optical Needles. *Photonics* **2024**, *11*, 203. [[CrossRef](#)]
27. Li, Q.K.; Chen, Q.D.; Niu, L.G.; Yu, Y.H.; Wang, L.; Sun, Y.L.; Sun, H.B. Sapphire-Based Dammann Gratings for UV Beam Splitting. *IEEE Photonics J.* **2016**, *8*, 2500208. [[CrossRef](#)]
28. Bhuyan, M.K.; Courvoisier, F.; Lacourt, P.A.; Jacquot, M.; Salut, R.; Furfaro, L.; Dudley, J.M. High Aspect Ratio Nanochannel Machining Using Single Shot Femtosecond Bessel Beams. *Appl. Phys. Lett.* **2010**, *97*, 081102. [[CrossRef](#)]
29. Gecys, P.; Dudutis, J.; Raciukaitis, G. Nanosecond Laser Processing of Soda-Lime Glass. *J. Laser Micro/Nanoeng.* **2015**, *10*, 254–258. [[CrossRef](#)]
30. Dharmavarapu, R.; Bhattacharya, S.; Juodkazis, S. Diffractive Optics for Axial Intensity Shaping of Bessel Beams. *J. Opt.* **2018**, *20*, 085606. [[CrossRef](#)]
31. Wang, Y.; Dou, W.; Meng, H. Vector Analyses of Linearly and Circularly Polarized Bessel Beams Using Hertz Vector Potentials. *Opt. Express* **2014**, *22*, 7821. [[CrossRef](#)]

**Disclaimer/Publisher's Note:** The statements, opinions and data contained in all publications are solely those of the individual author(s) and contributor(s) and not of MDPI and/or the editor(s). MDPI and/or the editor(s) disclaim responsibility for any injury to people or property resulting from any ideas, methods, instructions or products referred to in the content.